Borazine promoted growth of highly-oriented thin films

Koichi Tanaka[†,¶,*], Pedro Arias[†], Koki Hojo[†,‡], Tomoyasu Watanabe[†,‡], Michael E. Liao[†],
Angel Aleman[§], Hicham Zaid[†], Mark S. Goorsky[†], and Suneel Kodambaka[†,#]

[†]Department of Materials Science and Engineering, University of California Los Angeles, Los Angeles, CA 90095, USA
[§]Department of Mechanical and Aerospace Engineering, University of California Los Angeles, Los Angeles, CA 90095, USA
[‡]Graduate Department of Micro-Nano Mechanical Science and Engineering, Nagoya University, Furo-cho, Nagoya, Japan
[#]Department of Materials Science and Engineering, Virginia Polytechnic Institute and State University, Blacksburg, VA 24061, USA

[¶]Present Address; Pritzker School of Molecular Engineering, University of Chicago, Chicago, IL 60637
[*]Corresponding author

We report on a phenomenon, where thin films sputter-deposited on single-crystalline $Al_2O_3(0001)$ substrates exposed to borazine -- a precursor commonly used for the synthesis of hexagonal boron nitride layers -- are more highly-oriented than those grown on bare $Al_2O_3(0001)$ under the same conditions. We observed this phenomenon in face-centered cubic Pd, body-centered cubic Mo, and trigonal Ta_2C thin films grown on $Al_2O_3(0001)$. Interestingly, intermittent exposure to borazine during the growth of Ta_2C thin films on Ta_2C yields better crystallinity than direct deposition of monolithic Ta_2C. We attribute these rather unusual results to a combination of both enhanced adatom mobilities on, and epitaxial registry with, surfaces exposed to borazine during the deposition. We expect that our approach can potentially help improve crystalline quality of thin films deposited on a variety of substrates.

Crystallinity is an important characteristic that often dictates properties and life-time performance of materials. Microstructural evolution during the growth of thin films on solid substrates is often considered to be determined by two critical parameters, surface mass transport and deposition flux.[1] High fluxes and low diffusivity result in far-from-equilibrium microstructures while the opposite yield near-equilibrium, thermodynamically favorable microstructures. In general, by increasing substrate temperature (T_s) one can grow single-crystalline thin films by depositing at low rates. In practice, however, the depositing material may decompose, desorb, or react with the substrate upon increasing T_s.

An alternate approach to increasing T_s is *via* reducing substrate-deposit interactions. Three-dimensional (3D) substrate surfaces have dangling bonds that interfere with adatom diffusion. For epitaxial growth on such surfaces, lattice match between the film and the substrate is desirable. In contrast, van der Waals (vdW) surfaces, with weak out-of-plane bonds facilitate easy surface diffusion and 'free' nucleation. Koma and co-workers[2, 3] demonstrated over three decades ago that heteroepitaxial growth can be achieved without the need for lattice match using vdW-bonded materials (e.g., $NbSe_2/MoS_2$), which they referred to as vdW-epitaxy.[4-9] This concept was later extended to grow vdW layers on 3D solids [e.g., $MoSe_2/CaF_2(111)$],[10] *vice versa* [e.g., CdTe/WSe_2,],[11-14] 3D/3D using vdW buffer layers (e.g. GaAs/GaSe/Si, Cu/graphene/$Al_2O_3(0001)$),[15-18] and crystalline thin films on amorphous substrates with vdW buffer layers (e.g., CdTe/graphene/glass).[13, 19-22] Kim and co-workers reported on 'remote-epitaxy',[23, 24] homoepitaxial growth of GaN on graphene-covered single-crystalline GaN(001).[25-28] An important distinction between remote-epitaxy and vdW-epitaxy is that there exists definite crystallographic orientation relation between the film and the substrate in the former, whereas such requirement is relaxed in case of the latter.

Here, we present data that seemingly demonstrate a new phenomenon, wherein exposing the growth surfaces to borazine, a precursor used to grow hBN, yields thin films that are *more* highly oriented than homoepitaxially grown films. Our observations are not to be mistaken as vdW-epitaxy or remote-epitaxy, because neither of these phenomena have been associated with improvement in crystallinity of the deposits on substrates either covered with vdW buffer layers or exposed to precursors of such layers.

Using $Al_2O_3(0001)$ as a model substrate, chosen for its high thermochemical stability[29] and because hBN layers can be grown using borazine,[30] we tested the generality of this phenomenon using materials with different crystal structures and bonding: catalytically-active, face-centered-cubic (fcc) Pd, refractory body-centered-cubic (bcc) Mo and VNbTaMoW, and ultrahigh-temperature ceramics (trigonal-Ta_2C and B1-TaC) used in high-temperature structural applications. We chose VNbTaMoW because it is isostructural (bcc) to Mo with nearly the same lattice parameters[31] but is expected to be more sluggish and hence may exhibit different growth kinetics compared to Mo.

As a first step, we exposed $Al_2O_3(0001)$ substrates to borazine at high-temperatures. Experimental details and the results are summarized in Figure S1 of the Supporting Information (SI). Briefly, $Al_2O_3(0001)$ is exposed to 1.2×10^5 L borazine ($p_{\text{borazine}} = 2.0 \times 10^{-4}$ Torr for 600 s) at T_s = 1373 K. Based on Auger electron spectroscopy (AES) (Figure S1A) and low-energy electron diffraction (LEED) (Figures S1B, C) data acquired *in situ* from $Al_2O_3(0001)$ before and after exposure to borazine, we conclude that hBN layers form on $Al_2O_3(0001)$. From the LEED pattern in Figure S1C, we identify in-plane orientation of one of the hBN domains with respect to $Al_2O_3(0001)$ as $[10\bar{1}0]_{\text{hBN}} \parallel [2\bar{1}\bar{1}0]_{Al_2O_3}$. Although we detect hBN in both LEED and AES data from within ~1-mm-wide spot sizes across the sample, we do not know the exact thickness, size, or the areal coverage of the hBN domains. Raman spectroscopy and scanning transmission electron microscopy (STEM) data (details in the SI) of the borazine-exposed substrates before and after thin film deposition did not reveal any indication of hBN. Therefore, in the following sections, we use the notation (hBN) to indicate borazine-exposure.

All the metal (Mo, Pd, and VNbTaMoW) and compound (Ta_2C and TaC) thin films are grown on $Al_2O_3(0001)$ substrates at the desired T_s *via* ultra-high vacuum (UHV, base pressure < 6.0×10^{-9} Torr) direct current (dc) magnetron sputtering of the respective metal (Mo, Pd, and VNbTaMoW) and compound (TaC) targets[32-34] in a custom-designed, triple-source UHV deposition system.[35-37] All the experimental details are presented in the SI.

In the following sections, we compare and contrast the crystallinity of Ta_2C films grown on bare and borazine-covered $Al_2O_3(0001)$ substrates [hereafter referred to as (hBN)/$Al_2O_3(0001)$]. Figures 1A and S2 are representative LEED patterns obtained *in situ* from ~6-nm-thick Ta_2C layers sputter-deposited on (hBN)/$Al_2O_3(0001)$ and bare $Al_2O_3(0001)$, respectively. For Ta_2C on (hBN)/$Al_2O_3(0001)$, we find six-fold symmetric diffraction spots, which we attribute to the formation of highly ordered, smooth $Ta_2C(0001)$-(1×1) surface. In contrast, LEED pattern (see Figure S2) of $Ta_2C/Al_2O_3(0001)$ does not show any diffraction spots, suggestive of relatively poorer quality surface. Figure 1B shows typical 2θ-ω X-ray diffraction (XRD) scans, red and black curves, respectively obtained from the same set of samples. For $Ta_2C/Al_2O_3(0001)$, XRD data reveal only one peak at 2θ = 36.46° due to 0002 reflection of trigonal α-Ta_2C ($P\bar{3}m1$);[38] we note that this peak is not visible when the same data are plotted on linear scale, shown as inset in Figure 2B. In comparison, for $Ta_2C/(hBN)/Al_2O_3(0001)$, we see two peaks, at 2θ = 36.61° and 77.68°, respectively due to 0002 and 0004 reflections of α-Ta_2C, indicative of better crystallinity. The *c* values measured from the XRD data are comparable to those reported previously and deviations from the bulk value are to be expected in sputter-deposited Ta_2C thin films.[32, 34] We note that the 0002 peak appears broad with satellite peaks. As we show below, the Ta_2C layer on $(hBN)/Al_2O_3(0001)$ is single-crystalline and the satellite peaks are Laue oscillations associated with high-quality Ta_2C layers with abrupt interfaces. Normalized intensity I_{0002} of the α-Ta_2C 0002 peak, measured as a ratio of the α-Ta_2C 0002 and Al_2O_3 0006 peak intensities, is 3700× higher for $Ta_2C/(hBN)/Al_2O_3(0001)$ than for $Ta_2C/Al_2O_3(0001)$ sample. Clearly, borazine-exposure promotes highly 0001-oriented growth of Ta_2C layers.

Figures 1C and D are representative high-resolution bright-field TEM and high-angle annular dark-field STEM images, respectively acquired from the same $Ta_2C/(hBN)/Al_2O_3(0001)$ sample as in Figures 1A,B. The images and the Fourier transform (FT) in Figure 1C inset reveal highly-ordered lattice, indicative of single-crystallinity. From the FTs of the film and the substrate (not shown), we determine the orientation relation as $(0001)_{\mathrm{Ta_2C}} \parallel (0001)_{\mathrm{Al_2O_3}}$ and $[10\bar{1}0]_{\mathrm{Ta_2C}} \parallel [11\bar{2}0]_{\mathrm{Al_2O_3}}$; as we show later, Ta_2C layers deposited using the same parameters on bare $Al_2O_3(0001)$ bear the same orientation relationship, consistent with previous studies.[34] Furthermore, the STEM image in Figure 1D reveals uniform contrast across the thickness of the film, suggestive of compositional homogeneity in the film.

We provide additional evidence in support of this phenomenon in Figure S3, which shows XRD and XTEM data obtained from thicker (≈ 17 nm) $Ta_2C/(hBN)/Al_2O_3(0001)$ and $Ta_2C/Al_2O_3(0001)$ films deposited for t = 5 min. The 2θ-ω XRD scans in Figure S3A reveal that I_{0002} is over 17× higher for $Ta_2C/(hBN)/Al_2O_3(0001)$ than that for the $Ta_2C/Al_2O_3(0001)$ film. Furthermore, Laue oscillations around 0002 peak are observed in the XRD scan of the $Ta_2C/(hBN)/Al_2O_3(0001)$ but not in the other, indicative of higher crystalline quality of the film. XTEM image in Figure S3B and the associated FT in the inset of the $Ta_2C/(hBN)/Al_2O_3(0001)$ sample reveal that the layer is highly 0002-oriented. Electron energy loss spectra and energy dispersive spectra (not shown) acquired from the Ta_2C/(hBN)/Al_2O_3(0001) samples are inconclusive regarding the C content in the film and the presence of hBN layers at the interface. We speculate that the lack of direct evidence in support of the hBN layer could be due to decomposition of the hBN domains during sputter-deposition and/or due to the difficulty in distinguishing B and N atoms from C (in Ta_2C) and O (in Al_2O_3) atoms present at the interface. Nevertheless, the LEED pattern (Figure 1A), XRD scans (Figures 1B, S3A), along with TEM and STEM data (Figures 1C,D and S3B) all support the idea that borazine-exposed Al_2O_3(0001) substrates enhance the crystallinity and promote the growth of highly-oriented Ta_2C thin films.

We tested the generality of this phenomenon in the growth of materials with different crystal structures: 2H-MoS_2,[30] fcc-Pd,[37] bcc-Mo and VNbTaMoW, and B1-TaC. Figures 2A-D are typical 2θ-ω XRD scans obtained from A) Pd, B) Mo, C) VNbTaMoW, and D) TaC thin films sputter-deposited on bare Al_2O_3(0001) and (hBN)/Al_2O_3(0001). For the Pd/Al_2O_3(0001), Figure 2A shows high intensity peaks due to 111 and 222 Pd reflections, along with a peak due to Pd 220 reflection. For Mo/Al_2O_3(0001), we observe nearly equal intensity peaks associated with 110 and 222 reflections (Figure 2B). In comparison, XRD scans of Pd and Mo thin films on (hBN)/Al_2O_3(0001) substrates show peaks due to only one orientation, 111 and 222 reflections for Pd and 110 and 220 for Mo. For Mo/(hBN)/Al_2O_3(0001), pole figure in Figure S4 shows additional relatively weaker intensity spots due to 111-oriented grains. That is, with the same set of deposition parameters, we obtain polycrystalline Pd and Mo thin films on Al_2O_3(0001) and highly-oriented Mo(110) and Pd(111) layers on (hBN)/Al_2O_3(0001). XRD pole figures in Figure S4 provide further evidence in support of this claim.

In Figure 2C, XRD scans obtained from VNbTaMoW thin films indicate the growth of single-phase, bcc-structured alloy with 110 texture on both Al_2O_3(0001) and (hBN)/Al_2O_3(0001). We note the presence of both 110 and 220 peaks in the XRD scan from VNbTaMoW/Al_2O_3(0001) but only 110 peak in the XRD of VNbTaMoW/hBN/Al_2O_3(0001); the absence of 220 peak is likely due to poorer crystallinity of the film. XRD data in Figure 2D from TaC/Al_2O_3(0001) and TaC/(hBN)/Al_2O_3(0001) layers show B1-TaC 111 peaks with similar shapes and intensities. However, we do not observe any clear effect of hBN buffer layer on the TaC film crystallinity. The results presented in Figures 2C and D suggest that the phenomenon of borazine-promoted crystal growth is not universal and may not be applicable to all materials.

To understand the limitations of our approach, we carried out additional growth experiments using Ta_2C as the model material. We prepared three different types of Ta_2C samples labeled, *A*, *B*, and *C*, and their schematics are shown in Figure 3.

In Figure 3A, we compare and contrast XRD 2θ-ω scans obtained from Sample *A* with those from thinner Ta_2C/(hBN)/Al_2O_3(0001) layers deposited for $t = 2$ and 5 min., red curves in Figures 2B and S3A, respectively. The XRD and TEM data in Figures 2 and S3 indicate that the thinner samples are highly 0001-oriented. In contrast, XRD data from sample *A* reveal multiple peaks at 2θ = 38.35°, 59.62°, and 82.20°, respectively, corresponding to α-Ta_2C $10\bar{1}1$, $2\bar{1}\bar{1}0$, and $20\bar{2}2$ reflections, in addition to those due to α-Ta_2C $000l$, with $l = 2$, 3, and 4, reflections at 2θ = 36.30°, 55.72°, and 77.11°, respectively. That is, the monolithic Ta_2C films deposited for $t = 30$ min. are polycrystalline. These results reveal that under the same set of deposition conditions, Ta_2C layers grow heteroepitaxially for at least the first 5 minutes on (hBN)/Al_2O_3(0001); polycrystallinity develops in thicker Ta_2C films grown for $t = 30$ min.

We now present XRD 2θ-ω scans, solid green and blue curves, respectively, from samples *B* and *C* in Figure 4B. The XRD data for sample *B* shows primarily α-Ta_2C 0002 and 0004 reflections at 2θ = 36.27° and 77.03°, respectively. (We also observe weaker intensity peaks at 2θ around 34° and at ~73.2°, which are likely due to 111 and 222 reflections of B1-TaC.) XRD pole figure (Figure S5) obtained from this sample indicates that the Ta_2C is highly oriented with 0001 texture with the following orientation relationship with respect to Al_2O_3(0001): $(0001)_{Ta_2C} \parallel (0001)_{Al_2O_3}$ and $[10\bar{1}0]_{Ta_2C} \parallel [11\bar{2}0]_{Al_2O_3}$. XRD results from sample *C* show all the α-Ta_2C reflections at nearly the same 2θ values as in sample *A* and an additional peak at 2θ = 33.28° due to α-Ta_2C $10\bar{1}0$ reflection. That is, sample *C* is polycrystalline. So, while depositing Ta_2C layers on borazine-exposed Al_2O_3(0001) promotes 0001-oriented growth, continuous or intermittent deposition for longer times yield polycrystalline Ta_2C films. However, exposing to borazine at regular intervals continues to promote highly 0001-oriented α-Ta_2C growth.

Surprisingly, φ scans (see Figure 4C) acquired from the samples *A*, *B*, and *C* reveal that the Ta_2C films in all the three samples bear the *same* in-plane orientation, $[10\bar{1}0]_{Ta_2C} \parallel [11\bar{2}0]_{Al_2O_3}$, with underlying (hBN)/$Al_2O_3$(0001), as that observed (see the φ scan in Figure S6) in Ta_2C layers deposited using the same parameters on bare Al_2O_3(0001) for $t = 30$ min. (We find that this is also the case for Pd and Mo thin films, see Figure S4.) These results indicate that 0001-oriented Ta_2C

grains bear the *same* orientation relation with $Al_2O_3(0001)$ irrespective of the crystallinity (highly-oriented or polycrystalline) of the films grown with and without borazine exposure.

The above data in Figures 1, S3, and 3 indicate that borazine-exposure promotes heteroepitaxial growth of $Ta_2C(0001)$ on $Al_2O_3(0001)$, however, up to a certain thickness. Remarkably, continued Ta_2C deposition with or without interruptions on these heteroepitaxial $Ta_2C(0001)/(hBN)/Al_2O_3(0001)$ thin films result in polycrystalline Ta_2C. Highly 0001-oriented Ta_2C films can only be grown on borazine-exposed Ta_2C surfaces. To reiterate, under our deposition conditions, highly 0001-oriented growth of Ta_2C is observed on $(hBN)/Ta_2C(0001)$ surfaces but homoepitaxial growth of Ta_2C on $Ta_2C(0001)$ is not favored.

To explain these rather unusual results, we propose that borazine-exposure enhances surface mobilities of adspecies during deposition leading to nucleation and growth of highly-oriented crystalline thin films. While the exact mechanisms underlying this behavior are not clear, we envision two scenarios: i) borazine chemically modifies the surface but does not alter the surface structure. This is consistent with the fact that substrate-film orientation relationships are unaffected by borazine-exposure (see Figures 3, S4-S6). ii) Borazine decomposes to form hBN, a vdW layered material, that is likely to interact weakly with the deposit and hence promote surface diffusion. The latter is plausible especially on transition-metals[39, 40] and we have some evidence of hBN formation on $Al_2O_3(0001)$, see Figure S1. However, we do not know if borazine-exposure results in hBN formation on Ta_2C surfaces. In case there exists an hBN layer on the growth surfaces [$Al_2O_3(0001)$ and Ta_2C], then in order for the thin films to maintain the same in-plane orientation as those grown on bare $Al_2O_3(0001)$, either remote-epitaxy is operational or both the film and the hBN layer bear the same orientation relations with $Al_2O_3(0001)$. Our XRD pole figures along with LEED data from Figure 1 support such a possibility. We realize that this is rather unique and maybe specific to our growth conditions and the choice of materials.

Finally, we address the factors influencing the generality of the observed phenomena. As hypothesized above, weak interactions between the deposit and the vdW layer increase surface mobility of the adspecies resulting in highly-oriented film growth as is the case with Pd and Mo films on $(hBN)/Al_2O_3(0001)$ (Figures 2A, B). Qualitatively similar results have been reported for 2H-MoS_2 thin films reactively sputter-deposited on borazine-exposed $Al_2O_3(0001)$.[30] Given that 2H-MoS_2 is a vdW layered material, one would expect weak interactions between MoS_2 and $Al_2O_3(0001)$. Yet, results reported in Ref. [[30]] support the idea that borazine-exposure further weakens the interactions between MoS_2 and the substrate. However, stronger deposit/vdW-layer interactions can suppress surface mobility and affect the crystallinity. It is also possible that the substrate-deposit interactions, and hence mobilities of adspecies, are unaffected by the borazine-exposure under a given set of deposition conditions, in which case our approach will have little effect on the crystallinity of the deposited material (see for example Figures 2C, D). Therefore, we expect that the strength of surface/film interactions after borazine exposure, and hence the surface adatom mobilities, are likely to be material specific. Furthermore, it is to be seen if the observed enhancement in crystallinity is general and independent of substrate crystal orientation. That is, would similar heteroepitaxial growth occur for Pd or Ta_2C thin films, for example, on borazine-covered (001)-oriented substrates? Finally, it is to be determined whether similar phenomenon would be observed with precursors, e.g., ethylene, ammonium thiomolybdate, etc., respectively used for the growth of other vdW materials such as graphene and MoS_2, or even with mechanically-transferred hBN layers. Clearly, additional investigations of crystal growth on vdW surfaces,[41] for example *in situ* microscopy studies[42] of the nucleation and growth kinetics, are essential for understanding the mechanisms leading to vdW-epitaxy, remote-epitaxy, and the phenomena observed in our experiments.

In conclusion, we demonstrated an approach involving the use of borazine to enhance crystallinity and orientation of sputter-deposited thin films. Our approach yields highly-oriented fcc-Pd(111), bcc-Mo(110), and α-Ta_2C(0001) thin films on borazine-exposed Al_2O_3(0001) compared to those grown on bare Al_2O_3(0001) substrates. Sputter-deposition of bcc-VNbMoTaW and B1-TaC thin films on borazine-exposed Al_2O_3(0001) substrates did not yield similar results. A series of growth experiments conducted using Ta_2C revealed that the positive effect of borazine-exposure is limited to a finite film thickness beyond which polycrystallinity develops. We show that this issue can be overcome by intermittent exposure to borazine. Surprisingly, this approach facilitates epitaxial thin film growth under the deposition conditions that do not favor homoepitaxy. We attribute these observations to a combination of enhanced surface mobilities of the adspecies and epitaxial registry between the deposit and the substrate during sputter-deposition on surfaces exposed to borazine. While our observations maybe material-specific, we expect that similar enhancement in crystalline quality can be achieved in a variety of materials with the appropriate choice of the precursor and the deposition parameters.

AUTHOR CONTRIBUTIONS

S.K. and K.T. conceived the research. K.T. and P.A. conducted borazine depositions. K.T., H.Z., K.H., A.A., and T.W. synthesized and characterized sputter-deposited samples. K.T. and M.E.L. performed XRD under supervision from M.S. S.K. supervised and managed the project. S.K. and K.T. wrote the paper with contribution from all the authors. All authors discussed the results and analysis.

ASSOCIATED CONTENT

Supporting Information (SI): Additional LEED, AES, XRD, and TEM data of the borazine-exposures, Ta_2C thin films, and XRD pole figures of Pd and Mo thin films.

NOTES

The authors declare no competing financial interests.

ACKNOWLEDGEMENTS

We gratefully acknowledge support from the AFOSR (Dr. Ali Sayir) under Grant# FA9550-14-1-0106, FA9550-18-1-0050, and FA9550-20-1-0184, the NSF for Award# 2211350 (Dr. James Edgar), and the ONR (Dr. Chagaan Baatar) for Grant # N00014-12-1-0518. KT thanks the Japanese Student Service Organization (L16111111026) and the UCLA Department of Materials Science and Engineering for financial assistance. KH and TW are supported by the Japan US Advanced Collaborative Education Program (JUACEP). The authors acknowledge the use of facilities and instrumentation at the UC Irvine Materials Research Institute (IMRI), which is supported in part by the NSF through the UC Irvine Materials Research Science and Engineering Center (DMR-2011967). We thank Dr. Toshihiro Aoki for assistance with STEM and Mr. Noah Bodzin at the Nanoelectronics Research Facility in the UCLA Henry Samueli School of Engineering for assistance with FIB.

REFERENCES

1. Greene, J. E. Epitaxial Crystal Growth by Sputter Deposition: Applications to Semiconductors. Part 2. *Critical Reviews in Solid State and Materials Sciences* **1983,** 11 (3), 189-227.

2. Koma, A.; Sunouchi, K.; Miyajima, T. Fabrication and Characterization of Heterostructures with Subnanometer Thickness. *Microelectronic Engineering* **1984,** 2 (1), 129-136.

3. Koma, A. Summary Abstract: Fabrication of Ultrathin Heterostructures with Van Der Waals Epitaxy. *Journal of Vacuum Science & Technology B: Microelectronics and Nanometer Structures* **1985,** 3 (2).

4. Koma, A.; Yoshimura, K. Ultrasharp Interfaces Grown with Van Der Waals Epitaxy. *Surface Science* **1986,** 174 (1), 556-560.

5. Saiki, K.; Ueno, K.; Shimada, T.; Koma, A. Application of Van Der Waals Epitaxy to Highly Heterogeneous Systems. *Journal of Crystal Growth* **1989,** 95 (1), 603-606.

6. Ohuchi, F. S.; Parkinson, B. A.; Ueno, K.; Koma, A. Van Der Waals Epitaxial Growth and Characterization of Mose2thin Films on Sns2. *Journal of Applied Physics* **1990,** 68 (5), 2168-2175.

7. Koma, A. Van Der Waals Epitaxy - a New Epitaxial Growth Method for a Highly Lattice-Mismatched System. *Thin Solid Films* **1992,** 216, 72-76.

8. Koma, A. New Epitaxial Growth Method for Modulated Structures Using Van Der Waals Interactions. *Surface Science* **1992,** 267 (1), 29-33.

9. Koma, A. Van Der Waals Epitaxy for Highly Lattice-Mismatched Systems. *J. Cryst. Growth* **1999,** 201-202, 236-241.

10. Koma, A.; Saiki, K.; Sato, Y. Heteroepitaxy of a Two-Dimensional Material on a Three-Dimensional Material. *Appl. Surf. Sci.* **1990,** 41-42, 451-456.

11. Sun, X.; Lu, Z.; Xiang, Y.; Wang, Y.; Shi, J.; Wang, G. C.; Washington, M. A.; Lu, T. M. Van Der Waals Epitaxy of Antimony Islands, Sheets, and Thin Films on Single-Crystalline Graphene. *ACS Nano* **2018,** 12 (6), 6100-6108.

12. Löher, T.; Tomm, Y.; Klein, A.; Su, D.; Pettenkofer, C.; Jaegermann, W. Highly Oriented Layers of the Three‐Dimensional Semiconductor Cdte on the Two‐Dimensional Layered Semiconductors Mote2 and Wse2. *Journal of Applied Physics* **1996,** 80 (10), 5718-5722.

13. Mohanty, D.; Xie, W.; Wang, Y.; Lu, Z.; Shi, J.; Zhang, S.; Wang, G.-C.; Lu, T.-M.; Bhat, I. B. Van Der Waals Epitaxy of Cdte Thin Film on Graphene. *Applied Physics Letters* **2016,** 109 (14), 143109.

14. Littlejohn, A. J.; Xiang, Y.; Rauch, E.; Lu, T. M.; Wang, G. C. Van Der Waals Epitaxy of Ge Films on Mica. *Journal of Applied Physics* **2017,** 122 (18), 185305.

15. Palmer, J. E.; Saitoh, T.; Yodo, T.; Tamura, M. Growth and Characterization of Gaas/Gase/Si Heterostructures. *Jpn. J. Appl. Phys.* **1993,** 32 (Part 2, No. 8B), L1126-L1129.

16. Löher, T.; Ueno, K.; Koma, A. Van Der Waals Type Buffer Layers: Epitaxial Growth of the Large Lattice Mismatch System Cds/Inse/H–Si(111). *Appl. Surf. Sci.* **1998,** 130-132, 334-339.

17. Löher, T.; Koma, A. Epitaxial Growth of Znse on Si(111) with Lattice-Matched Layered Inse Buffer Layers. *Jpn. J. Appl. Phys.* **1998,** 37 (Part 2, No. 9A/B), L1062-L1064.

18. Lu, Z.; Sun, X.; Xie, W.; Littlejohn, A.; Wang, G.-C.; Zhang, S.; Washington, M. A.; Lu, T.-M. Remote Epitaxy of Copper on Sapphire through Monolayer Graphene Buffer. *Nanotechnology* **2018,** 29 (44), 445702.

19. Saito, Y.; Fons, P.; Kolobov, A. V.; Tominaga, J. Self-Organized Van Der Waals Epitaxy of Layered Chalcogenide Structures. *physica status solidi (b)* **2015,** 252 (10), 2151-2158.

20. Sun, X.; Chen, Z.; Wang, Y.; Lu, Z.; Shi, J.; Washington, M.; Lu, T.-M. Van Der Waals Epitaxial Znte Thin Film on Single-Crystalline Graphene. *Journal of Applied Physics* **2018,** 123 (2), 025303.

21. Sun, X.; Lu, Z.; Xie, W.; Wang, Y.; Shi, J.; Zhang, S.; Washington, M. A.; Lu, T.-M. Van Der Waals Epitaxy of Cds Thin Films on Single-Crystalline Graphene. *Applied Physics Letters* **2017,** 110 (15), 153104.

22. Rajbhandari, P. P.; Chaudhari, A.; Dhakal, T. P. Substrate Independent Oriented 2d Growth of Sns Thin Films from Sputtering. *Materials Research Express* **2019,** 6 (11), 116427.

23. Kim, Y.; Cruz, S. S.; Lee, K.; Alawode, B. O.; Choi, C.; Song, Y.; Johnson, J. M.; Heidelberger, C.; Kong, W.; Choi, S.; Qiao, K.; Almansouri, I.; Fitzgerald, E. A.; Kong, J.; Kolpak, A. M.; Hwang, J.; Kim, J. Remote Epitaxy through Graphene Enables Two-Dimensional Material-Based Layer Transfer. *Nature* **2017,** 544 (7650), 340-343.

24. Kong, W.; Li, H.; Qiao, K.; Kim, Y.; Lee, K.; Nie, Y.; Lee, D.; Osadchy, T.; Molnar, R. J.; Gaskill, D. K.; Myers-Ward, R. L.; Daniels, K. M.; Zhang, Y.; Sundram, S.; Yu, Y.; Bae, S. H.; Rajan, S.; Shao-Horn, Y.; Cho, K.; Ougazzaden, A.; Grossman, J. C.; Kim, J. Polarity Governs Atomic Interaction through Two-Dimensional Materials. *Nat Mater* **2018,** 17 (11), 999-1004.

25. Jeong, J.; Jin, D. K.; Cha, J.; Kang, B. K.; Wang, Q.; Choi, J.; Lee, S. W.; Mikhailovskii, V. Y.; Neplokh, V.; Amador-Mendez, N.; Tchernycheva, M.; Yang, W. S.; Yoo, J.; Kim, M. J.; Hong, S.; Hong, Y. J. Selective-Area Remote Epitaxy of Zno Microrods Using Multilayer–Monolayer-Patterned Graphene for Transferable and Flexible Device Fabrications. *ACS Applied Nano Materials* **2020**.

26. Jia, R.; Kum, H. S.; Sun, X.; Guo, Y.; Wang, B.; Fang, P.; Jiang, J.; Gall, D.; Lu, T.-M.; Washington, M.; Kim, J.; Shi, J. Van Der Waals Epitaxy and Remote Epitaxy of Linbo3 Thin Films by Pulsed Laser Deposition. *Journal of Vacuum Science & Technology A* **2021,** 39 (4).

27. Journot, T.; Okuno, H.; Mollard, N.; Michon, A.; Dagher, R.; Gergaud, P.; Dijon, J.; Kolobov, A. V.; Hyot, B. Remote Epitaxy Using Graphene Enables Growth of Stress-Free Gan. *Nanotechnology* **2019,** 30 (50), 505603.

28. Lu, Z.; Sun, X.; Xie, W.; Littlejohn, A.; Wang, G. C.; Zhang, S.; Washington, M. A.; Lu, T. M. Remote Epitaxy of Copper on Sapphire through Monolayer Graphene Buffer. *Nanotechnology* **2018,** 29 (44), 445702.

29. Kodambaka, S.; Israeli, N.; Bareno, J.; Swiech, W.; Ohmori, K.; Petrov, I.; Greene, J. E. Low-Energy Electron Microscopy Studies of Interlayer Mass Transport Kinetics on Tin(111). *Surface Science* **2004,** 560 (1-3), 53-62.

30. Aryeetey, F.; Ignatova, T.; Aravamudhan, S. Quantification of Defects Engineered in Single Layer Mos2. *RSC Advances* **2020,** 10 (39), 22996-23001.

31. Zaid, H.; Stremfel, J. W.; Tanaka, K.; Liao, M.; Goorsky, M. S.; Yang, J.-M.; Kodambaka, S. Mechanical Properties of Compositionally-Rich Body-Centered Cubic Vnbtamow Alloy. *Materialia* **2020,** 12, 100746.

32. Tanaka, K.; Aleman, A.; Liao, M. E.; Wang, Y.; Goorsky, M. S.; Kodambaka, S. Effects of Ultra-Low Ethylene Partial Pressure on Microstructure and Composition of Reactively Sputter-Deposited Ta–C Thin Films. *Thin Solid Films* **2019,** 688, 137440.

33. Tanaka, K.; Liao, M. E.; Aleman, A.; Zaid, H.; Goorsky, M. S.; Kodambaka, S. Growth of Heterolayered [Cubic-Tac(111) + rhombohedral-Ta3c2(0001)] Nanocomposite Thin Films on Al2o3(0001). *Acta Mater.* **2021,** 204, 116499.

34. Tanaka, K.; Aleman, A.; Zaid, H.; Liao, M. E.; Hojo, K.; Wang, Y.; Goorsky, M. S.; Kodambaka, S. Ultra-High Vacuum Dc Magnetron Sputter-Deposition of 0001-Textured Trigonal A-$Ta_2c/Al_2o_3(0001)$ Thin Films. *Materialia* **2020,** 13, 100838.

35. Fankhauser, J.; Sato, M.; Yu, D.; Ebnonnasir, A.; Kobashi, M.; Goorsky, M. S.; Kodambaka, S. Growth and Characterization of Epitaxial Zr(0001) Thin Films on $Al_2o_3(0001)$. *Journal of Vacuum Science & Technology A* **2016,** 34 (5), 050606.

36. Tanaka, K.; Fankhauser, J.; Zaid, H.; Aleman, A.; Sato, M.; Yu, D.; Ebnonnasir, A.; Li, C.; Kobashi, M.; Goorsky, M. S.; Kodambaka, S. Kinetics of Zr-Al Intermetallic Compound Formation During Ultra-High Vacuum Magnetron Sputter-Deposition of $Zr/Al_2o_3(0001)$ Thin Films. *Acta Mater.* **2018,** 152, 34-40.

37. Aleman, A.; Li, C.; Zaid, H.; Kindlund, H.; Fankhauser, J.; Prikhodko, S. V.; Goorsky, M. S.; Kodambaka, S. Ultrahigh Vacuum Dc Magnetron Sputter-Deposition of Epitaxial Pd(111)/Al2o3(0001) Thin Films. *Journal of Vacuum Science & Technology A: Vacuum, Surfaces, and Films* **2018,** 36 (3), 030602.

38. Bowman, A. L.; Wallace, T. C.; Yarnell, J. L.; Wenzel, R. G.; Storms, E. K. The Crystal Structures of V_2c and Ta_2c. *Acta Crystallographica* **1965,** 19, 6.

39. Arias, P.; Abdulslam, A.; Ebnonnasir, A.; Ciobanu, C. V.; Kodambaka, S. Bifurcation and Orientation-Dependence of Corrugation of 2d Hexagonal Boron Nitride on Palladium. *2D Materials* **2018,** 5 (4), 045001.

40. Arias, P.; Ebnonnasir, A.; Ciobanu, C. V.; Kodambaka, S. Growth Kinetics of Two-Dimensional Hexagonal Boron Nitride Layers on Pd(111). *Nano Lett.* **2020,** 20 (4), 2886-2891.

41. Xin, W.; Severino, J.; De Rosa, I. M.; Yu, D.; McKay, J.; Ye, P.; Yin, X.; Yang, J.-M.; Carlson, L.; Kodambaka, S. One-Step Synthesis of Tunable-Size Gold Nanoplates on Graphene Multilayers. *Nano Lett.* **2018,** 18 (3), 1875-1881.

42. Mok, H. S.; Ebnonnasir, A.; Murata, Y.; Nie, S.; McCarty, K. F.; Ciobanu, C. V.; Kodambaka, S. Kinetics of Monolayer Graphene Growth by Segregation on Pd(111). *Applied Physics Letters* **2014,** 104 (10), 101606.

Figures

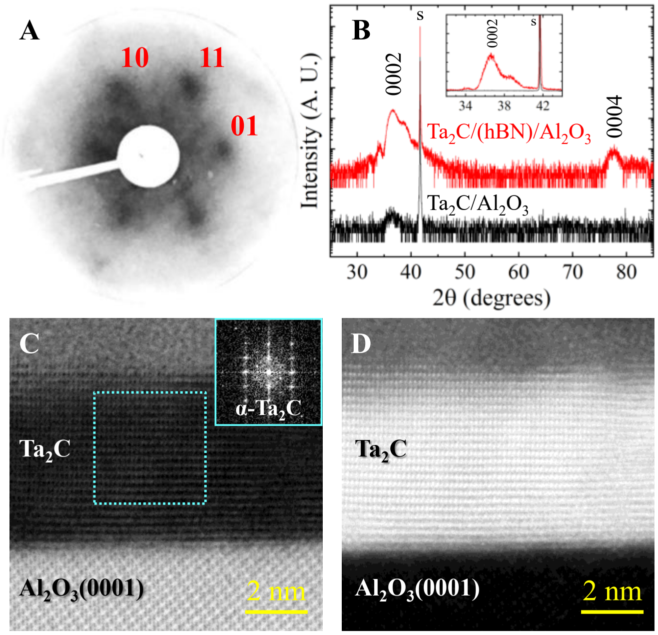

Figure 1. (**A**) Representative LEED pattern, (**B**) 2θ-ω XRD scan (red curve), and (**C**) bright field and (**D**) high-angle annular dark field cross-sectional TEM images obtained from an ~ 6-nm-thick Ta_2C/(hBN)/Al_2O_3(0001) film. Black curve in **B** is an XRD scan obtained from Ta_2C/Al_2O_3(0001). LEED pattern of this Ta_2C/Al_2O_3(0001) is shown in Figure S2. Intensities in each of the XRD curves are normalized to those of the Al_2O_3 0006 reflections (labeled **s**) and are plotted on a logarithmic scale. Ta_2C film reflections are labeled as shown. Inset in **B** shows the same XRD data plotted with intensities on linear scale. Inset in **C** is a Fourier transform (FT) of the region highlighted by a cyan-dotted square in **C**. From the observed symmetry of the reflections, we determine the zone axis as $[10\bar{1}0]_{Ta_2C}$ and index all the observed reflections as due to $\{000\ 2l\}$, $\{11\bar{2}\ 2l\}$, and $\{\bar{1}\bar{1}2\ 2l\}$ planes. In this experiment, Ta_2C is sputter-deposited for $t = 2$ min. at T_s = 1373 K and hBN layers are grown using borazine ($p_{\text{borazine}} = 2.0 \times 10^{-4}$ Torr) for $t = 10$ min. at the same T_s. Incident electron beam energy E used for LEED is 214 eV.

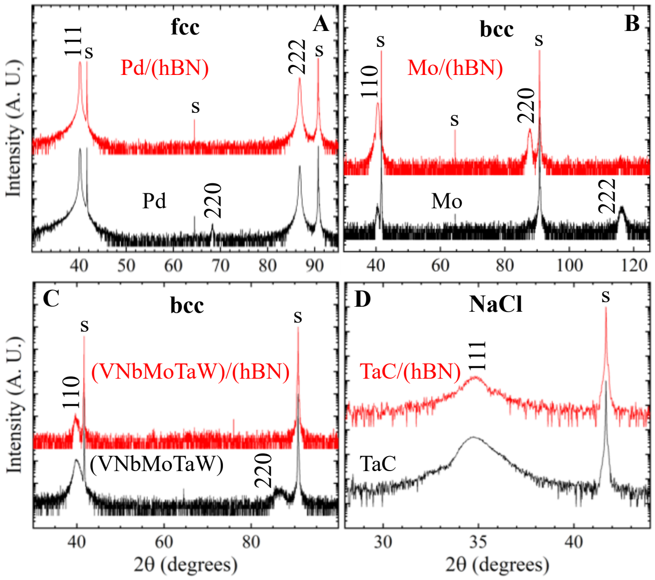

Figure 2. XRD 2θ-ω scans, with intensities normalized to those of the Al_2O_3 0006 reflections and plotted on a logarithmic scale, obtained from (A) Pd, (B) Mo, (C) VNbMoTaW, and (D) TaC thin films deposited on (hBN)/Al_2O_3(0001) (red curves) and bare Al_2O_3(0001) (black curves), following the procedure described in the SI. Al_2O_3 000*l* (with *l* = 6, 9, and 12) reflections are denoted by s.

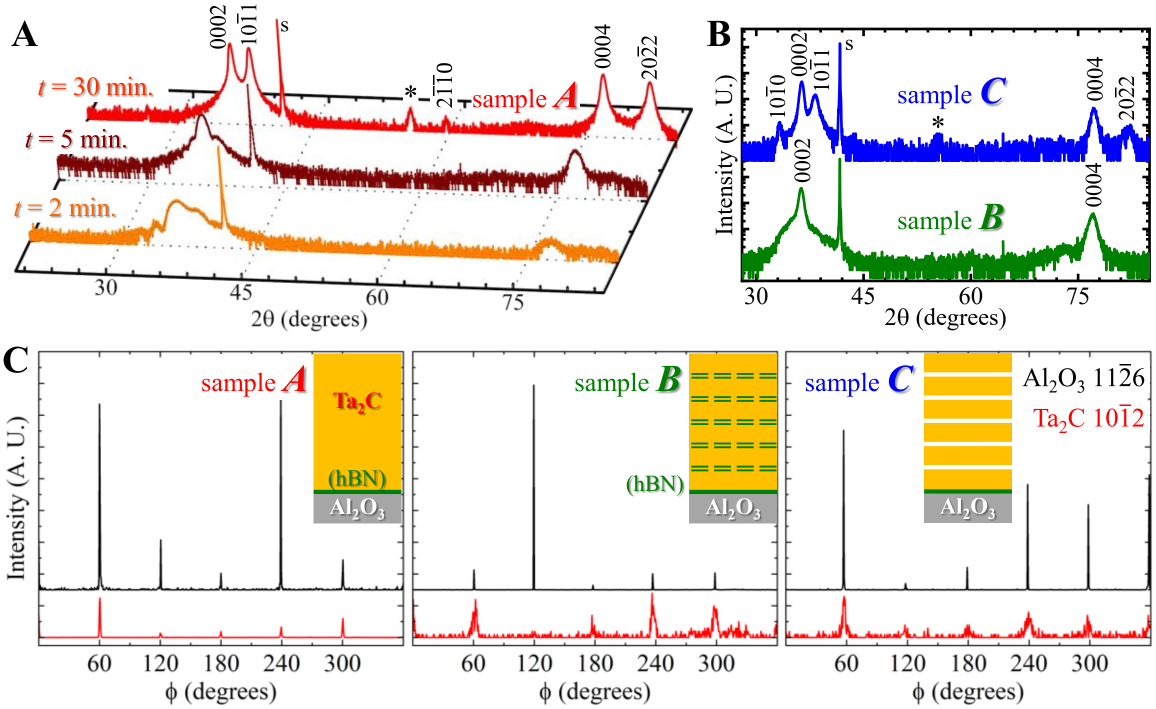

Figure 3. (**A**, **B**) Typical XRD 2θ-ω scans, with intensities normalized to those of the Al$_2$O$_3$ 0006 reflections and plotted on a logarithmic scale, obtained from: (**A**) Ta$_2$C thin films deposited for t = 2, 5, and 30 min. (sample A) on (hBN)/Al$_2$O$_3$(0001) and (**B**) samples B and C. s denotes Al$_2$O$_3$ 0006 reflections. Asterisk indicates a peak, likely due to α-Ta$_2$C 0003 reflection. (**C**) XRD phi scans of (red curves) Ta$_2$C 10$\bar{1}$2 and (black curves) Al$_2$O$_3$ 11$\bar{2}$6 reflections from samples A, B, and C, schematics of which are shown as insets. A, B, and C are all grown on borazine-exposed Al$_2$O$_3$(0001) substrates using the same parameters for the *same* total time t = 30 min. Sample A is a relatively thick Ta$_2$C film deposited on (hBN)/Al$_2$O$_3$(0001) without any interruptions for t = 30 min. Sample B is made of six Ta$_2$C thin films, with each layer sputter-deposited for t = 5 min. after exposure to borazine with $p_{\text{borazine}} = 1.0 \times 10^{-6}$ Torr for 10 min at the same T, i.e. sample $B \equiv$ 5×[Ta$_2$C/(hBN)]/Ta$_2$C/(hBN)/Al$_2$O$_3$(0001). The total time elapsed between each Ta$_2$C deposition due to borazine exposure is 15 min. Sample C is also made of six Ta$_2$C layers as in B with each layer grown for t = 5 min., but instead of exposing the surfaces to borazine, the sample is held in 20 mTorr Ar at the same T for 15 min., i.e. the same time as required for the borazine exposures in sample B. The observed differences in relative peak intensities within the phi scans are due to differences in effective irradiation of the X-ray beam during data acquisition and are not indicative of sample quality.